Measurement-Based Modeling of Vehicle-to-Vehicle MIMO Channels

Johan Karedal,[1] *Student Member, IEEE*, Fredrik Tufvesson,[1] *Senior Member, IEEE*, Nicolai Czink,[2] *Student Member, IEEE*, Alexander Paier,[3] *Student Member, IEEE*, Charlotte Dumard,[3] Thomas Zemen,[4] *Member, IEEE*, Christoph F. Mecklenbräuker,[4] *Senior Member, IEEE* and Andreas F. Molisch,[1,5] *Fellow, IEEE*

[1]Dept. of Electrical and Information Technology, Lund University, Lund, Sweden.
[2]Stanford University, Stanford, CA, USA.
[3]Inst. für Nachrichtentechnik und Hochfrequenztechnik, Technische Universität Wien, Vienna, Austria.
[4]Forschungszentrum Telekommunikation Wien (ftw.), Vienna, Austria.
[5]Mitsubishi Electric Research Laboratories (MERL), Cambridge, MA, USA.

***Abstract*— Vehicle-to-vehicle (VTV) communications are of interest for applications within traffic safety and congestion avoidance, but the development of suitable communications systems requires accurate models for VTV propagation channels. This paper presents a new wideband MIMO (multiple-input-multiple-output) channel model for VTV channels based on extensive MIMO channel measurements performed at 5.2 GHz in rural environments in Lund, Sweden. The measured channel characteristics, in particular the non-stationarity of the channel statistics, motivate the use of a geometry-based stochastic channel model (GSCM) instead of the classical tapped-delay line model. We introduce generalizations of the generic GSCM approach and find it suitable to distinguish between diffuse and discrete scattering contributions. The time-variant contributions from discrete scatterers are tracked over time and delay using a high resolution algorithm, and our observations motivate their power being modeled as a combination of a deterministic part and a stochastic part. The paper gives a full model parameterization and the model is verified by comparison of MIMO antenna correlations derived from the channel model to those obtained directly from measurements.**

I. Introduction

Wireless vehicle-to-vehicle (VTV) communications has recently received a lot of attention, with applications envisioned to reduce traffic accidents and facilitate traffic flow [1]. As with many wireless systems under development, the use of multiple antennas (MIMO) is of interest to enhance reliability and capacity of the VTV link [2], [3], [4], [5].

It is well-known that wireless system design requires knowledge about the propagation channel characteristics in which the envisioned system will operate. However, up to this point few investigations have considered modeling of MIMO VTV channels and there exists, to the author's best knowledge, no current MIMO model fully able to describe the time-varying nature of the VTV channel reported in measurements [6].

Generally speaking, there are three fundamental approaches to channel modeling: deterministic, stochastic, and geometry-based stochastic [7], [8]. The deterministic approach of VTV modeling has been explored extensively by Wiesbeck and co-workers [9], [10] and shown to agree well with (single-antenna) measurements. However, its main drawback is the requirement for intensive computations which also makes it difficult to vary propagation parameters. Stochastic channel models provide the statistics of the power received with a certain delay, Doppler shift, angle-of-arrival etc. A tapped delay-Doppler profile model was developed for the VTV channel, by Ingram and coworkers [11], [12], however, the assumption of a fixed Doppler spectrum for every delay does not represent the non-stationary channel responses reported in measurements [6].

Geometry-based stochastic channel models (GSCMs) [13], [14] have previously been found well suited for non-stationary environments [15], [16], and is the type of model we aim for in this paper. GSCMs build on placing scatterers at random, according to a certain statistical distribution, and assigning them (scattering) properties. Then the signal contributions of the scatterers are determined from a greatly-simplified ray tracing, followed by a summation of the total signal at the receiver. This modeling approach has a number of important benefits: (i) it can easily handle non-WSSUS channels, (ii) it provides not only delay and Doppler spectra, but inherently models the MIMO properties of the channel, (iii) it is possible to easily change the antenna influence, by simply including a different antenna pattern, (iv) the environment can be easily changed, and (v) it is much faster than deterministic ray tracing, since only single (or double) scattering needs to be simulated. A few geometrical VTV models with scatterers placed on *regular* shapes have been proposed, e.g., [17], however, their underlying assumption of all scatterers being static does not agree with results reported in measurements [18]. In this paper, we present a GSCM for MIMO VTV channels based on a more *realistic* placement of static *and* dynamic scatterers and parameterize it using results from an extensive measurement campaign on rural roads near Lund, Sweden.

The main contributions of this paper are the following:

- We develop a generic modeling approach for VTV channels based on GSCM. In this context, we extend existing GSCM structures by prescribing fading characteristics for specific scatterers.
- Based on the extracted scatterer contributions, we parameterize the generic channel model.
- We verify our parameterized model by comparing MIMO

This work was partially funded by the SSF Center of Excellence for High-Speed Wireless Communications (HSWC), the competence center program COMET, WWTF in the ftw. projects I0 and I2 and COST 2100.

correlation matrices as obtained from our model to directly measured ones.

The remainder of the paper is organized as follows: Sec. II briefly describes the measurement campaign for vehicle-to-vehicle MIMO channels that serves as the motivation for our modeling approach and Sec. III points out the most important channel characteristics to be included in the model. The channel model is described in Sec. IV and Sec. V compares the model outcomes with the measured results. Finally, a summary and conclusions in Sec. VI wraps up the paper.

II. Vehicle-to-Vehicle MIMO Channel Measurements

A. Measurement Setup

VTV channel measurements were performed with the RUSK LUND channel sounder that performs MIMO measurements based on the "switched array" principle [19] and records the time-variant complex channel transfer function $H(t, f)$. A frequency range of 5.2 ± 0.12 GHz was used for the measurements and with a test signal length of 3.2 μs we had a path resolution of 1.25 m and a maximum path delay of 959 m. The channel was sampled every 0.3072 ms, during a time window of roughly 10 s implying a maximum resolvable Doppler shift of 1.6 kHz, corresponding to a relative speed of 338 km/h at 5.2 GHz.

Transmitter (TX) and receiver (RX) were mounted on the platforms of separate pickup trucks (at a height of approximately 2.4 m above the street level), each consisting of a $4-$element, vertically polarized, circular microstrip antenna array mounted so that the broadside directions of the antenna elements were directed at 45, 135, 225 and 315 degrees, where 0 degrees denotes the direction of travel, respectively. Thus, a 4×4 MIMO system was measured.

We performed measurements on a rural motorway located near Lund, Sweden (see [20] for analysis of a highway scenario). The surroundings are mainly characterized by roadside fields, along with some sparsely scattered residential houses, farm houses and road signs. Little to no traffic prevailed during the measurements.

Measurements were performed both with TX and RX driving in the same direction (SM), and with TX and RX driving in opposite directions (OP). During each measurement, the aim was to maintain the same speed for TX and RX, though this speed was varied between different measurements in order to obtain a larger statistical ensemble. Also, the distance between TX and RX was kept approximately constant during each SM measurement, though it varied between different measurements. 32 SM and 12 OP measurements were performed.

III. VTV Channel Characteristics

A. Time-Delay Domain

Average power delay profiles (APDPs) were obtained by inverse discrete Fourier transforming the recorded frequency responses $H(t, f)$, using a Hanning window to suppress side lobes, and averaging the squared magnitudes of the resulting impulse responses $h(t, \tau)$ over a sample time corresponding to a TX movement of 20λ. We draw the following conclusions from the time-delay domain results (see Fig. 1 for a typical sample plot): (i) the LOS path is always strong, (ii) significant energy is available through discrete components, typically represented by a single tap (e.g., the diagonal "lines" in Fig. 1), (iii) discrete components typically move through many delay bins during a measurement; this implies that the common assumption of WSSUS is violated [18], (iv) discrete components may stem from mobile as well as static scattering objects, and (v) the LOS is usually followed by a tail of weak components. Analysis of the amplitude statistics of the taps immediately following the LOS tap shows that they can be well described by a Rayleigh distribution [20].

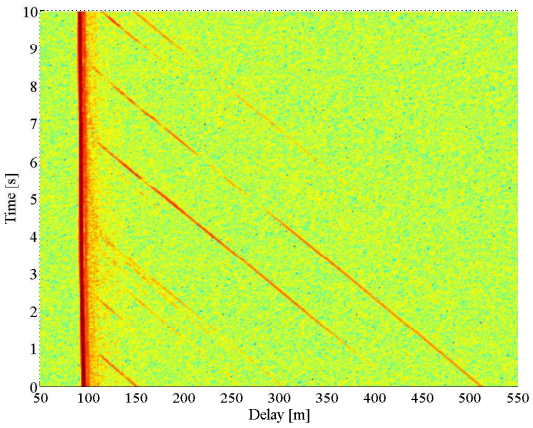

Fig. 1. Example plot of the time-varying APDP of a SM measurement (the approximate TX/RX speed was 90 km/h). Several reflections from discrete scatterers, all static, are visible as diagonal lines.

B. Delay-Doppler Domain

Doppler-resolved impulse responses, $h(\nu, \tau)$, were derived by Fourier transforming $h(t, \tau)$ with respect to t. The following conclusions are drawn: (i) the total Doppler spectrum can change significantly during a measurement, as scatterers change their position and speed relative to TX and RX, (ii) the Doppler spread of discrete scatterers is typically small, (iii) the tail of weak components not only has a large delay spread, but also a large Doppler spread. In the sequel, we denote this part of the channel "diffuse" in order to distinguish it from the discrete components.

Assuming single reflections only, simple geometric relations provide the relationship between angles of arrival/departure and scatterer velocity and thus can tell us whether a scatterer is mobile or static. We also note that the Doppler shifts produced by scattering points on a line parallel to the direction of travel closely matches the Doppler characteristics of the tail of diffuse components (for details, see [20]).

C. Discrete Scatterer Contribution

Analyzing the time-varying signal contribution of the discrete scatterers, such as the diagonal "lines" of Fig. 1, provides further insight into the propagation mechanisms. This is achieved using an algorithm of two steps, briefly summarized

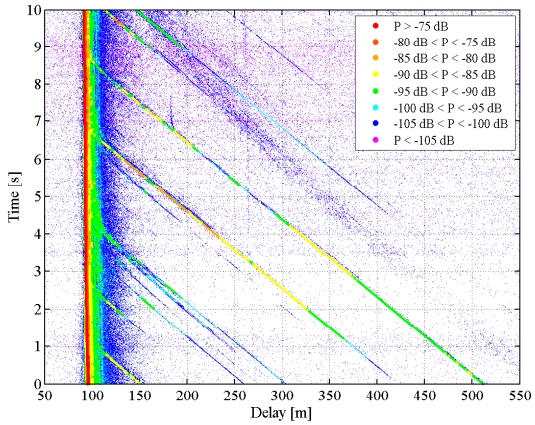

Fig. 2. High resolution impulse response of the measurement in Fig. 1.

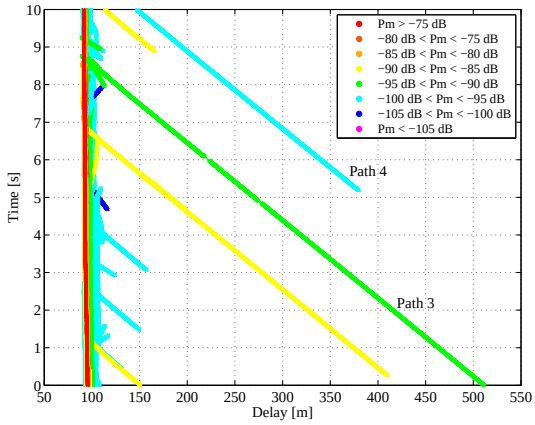

Fig. 3. Extracted paths from Fig. 2 after the second step of the algorithm.

below (the full algorithm is described in [20]). We first estimate the delays τ_i and amplitudes a_i of each multipath contribution at each time instant separately, by means of a high-resolution approach that is based on a serial "search-and-subtract" approach (similar to the CLEAN method [21]). We then perform tracking of the time-varying delay and power of the components over large timescales, utilizing the fine temporal increment of the measurements. Figs. 2 and 3 show the outcome of the first and second part of the algorithm, respectively.

Tracking the discrete components over time and distance (see Fig. 4 for an example) shows that their contributions are fading, likely due to one or several (unresolvable) ground reflections. We thus find that the standard GSCM way of modeling the complex path amplitudes as non-fading is not well suited for this type of reflections.

IV. A Geometry-Based Stochastic MIMO Model

A. General Model Outline

We define a geometry as in Fig. 5, where we distinguish between three types of point scatterers: mobile discrete, static discrete, and diffuse. Then, the double-directional, time-variant, complex impulse response of the channel is given as the superposition of the N paths (contributions from scatterers)

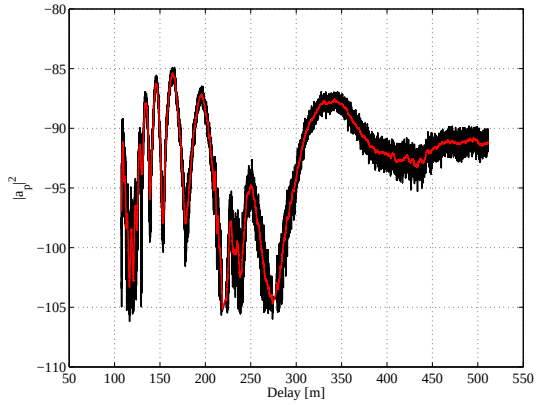

Fig. 4. Power as function of propagation distance for Path 3 of Fig. 3. In the figure is also plotted the low-pass filtered signal (red).

[16], i.e.,

$$h\left(t,\tau,\right)=\sum_{i=1}^{N}a_i e^{jkd_i(t)}\delta\left(\tau-\tau_i\right)\times\delta\left(\Omega_R-\Omega_{R,i}\right)\delta\left(\Omega_T-\Omega_{T,i}\right)g_R(\Omega_R)g_T(\Omega_T),\quad(1)$$

where τ_i, $\Omega_{R,i}$, and $\Omega_{T,i}$ are the excess delay, angle-of-arrival (AOA), and angle-of-departure (AOD) of path i, $g_T\left(\Omega_T\right)$ and $g_R\left(\Omega_R\right)$ are the TX and RX antenna patterns respectively, a_i is the complex amplitude associated with path i, $e^{jkd_i(t)}$ the corresponding distance-induced phase shift, and $k=2\pi\lambda^{-1}$ is the wave number. Channel coefficients for all branches of a MIMO system are easily obtained by summing up all channel contributions according to (1) at the positions of the respective antenna elements, using the appropriate antenna patterns [22].

In agreement with our measurement results, the impulse response of (1) is divided into four parts: (i) the LOS component, (ii) discrete components stemming from reflections off mobile scatterers (MD), (iii) discrete components stemming from reflections off static scatterers (SD) and (iv) diffuse components (DI). We thus have (omitting the AOA and AOD notation for convenience)

$$h\left(t,\tau\right)=h_{\mathrm{LOS}}\left(t,\tau\right)+\sum_{p=1}^{P}h_{\mathrm{MD}}\left(t,\tau_p\right)+\sum_{q=1}^{Q}h_{\mathrm{SD}}\left(t,\tau_q\right)+\sum_{r=1}^{R}h_{\mathrm{DI}}\left(t,\tau_r\right),\quad(2)$$

where P is the number of mobile discrete scatterers, Q is the number of static discrete scatterers and R is the number of diffuse scatterers. We assume single-reflections only,[1] and hence the propagation distance $d(t)$ is immediately given by the geometry at any time instant t for reflected paths as well as the LOS path. Furthermore, based on our observations in Sec. III-C, we assume that the complex amplitudes of the LOS path as well as the *discrete* scatterers are fading, i.e., $a_{\mathrm{LOS}}=a_{\mathrm{LOS}}\left(d\right)$, $a_p=a_p\left(d\right)$ and $a_q=a_q\left(d\right)$, which is in contrast to conventional GSCM modeling. With this strategy,

[1] A more thorough discussion on this and further assumptions, as well as their justifications, can be found in [20].

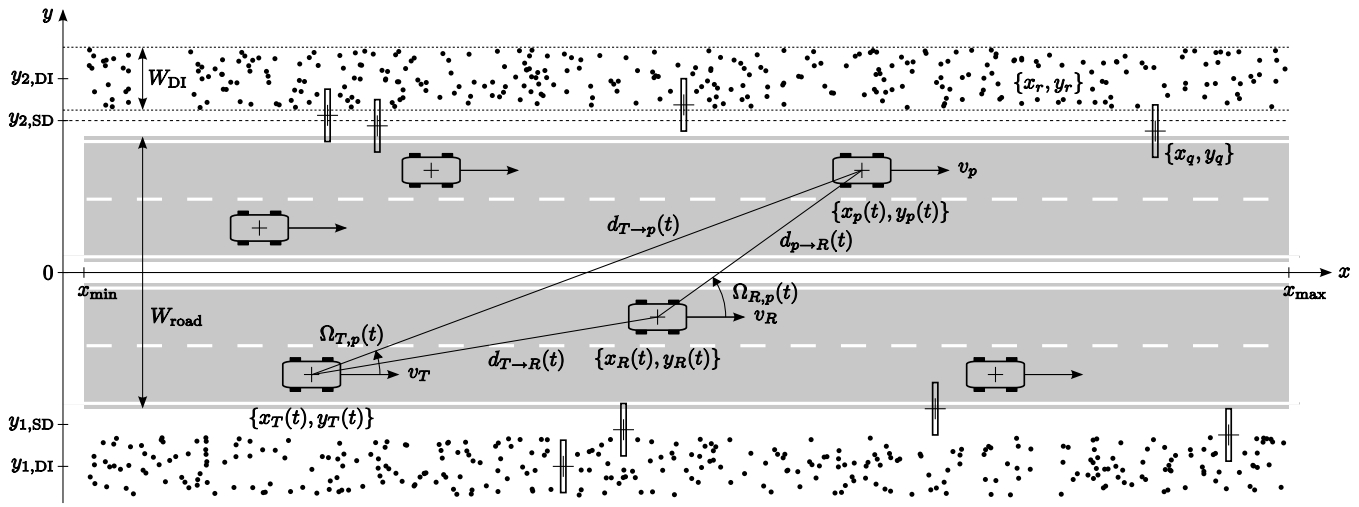

Fig. 5. Geometry for the VTV channel model. A transmitter with coordinates $\{x_T(t), y_T(t)\}$, moving at a speed v_T in the direction of the x–axis, is communicating with a receiver with coordinates $\{x_R(t), y_R(t)\}$, moving at a speed v_R. Scatterers are present as three types: mobile discrete scatterers (other vehicles) with coordinates $\{x_p(t), y_p(t)\}$ and a speed v_p, static discrete scatterers (road signs and other significant scattering points; in the figure drawn as road signs only) with coordinates $\{x_q(t), y_q(t)\}$ and (static) diffuse scatterers (represented as dots) with coordinates $\{x_r, y_r\}$.

we thus incorporate the combined contributions of several (unresolvable) paths into a single parameter. The complex amplitudes of the diffuse scattering points are modeled as in standard GSCM.

B. Path Amplitudes

1) Discrete Scatterers: For a discrete scatterer p, we divide the complex amplitude a_p into a deterministic (distance-decaying) part and a stochastic part, i.e.,

$$a_p\left(d_p\right) = g_S e^{j\phi_p} G_{0,p}^{1/2} \left(\frac{d_{\text{ref}}}{d_{T\to p} + d_{p\to R}}\right)^{n_p/2}, \qquad (3)$$

where $G_{0,p}$ is the received power at a reference distance d_{ref}, n_p is the pathloss exponent, ϕ_p is the phase shift due to the scatterer, and g_S is the real-valued, slowly varying,[2] stochastic amplitude gain of the scatterer (note that this representation is similar to the classical model for, narrowband, pathloss [22]). We stress that even though the model is the same for mobile and static scatterers, we provide separate sets of model parameters for each.[3] The same model also applies for the LOS component (with the subindex p replaced by LOS).

The phase ϕ_p is found to be only *slowly* varying, a phenomenon we subscribe to phase drift of the TX/RX oscillators and noise. We therefore leave out any stochastic phase modeling and instead follow the classical GSCM approach of giving the discrete scatterers a uniformly distributed random phase shift, i.e., $\phi \sim \mathcal{U}\left(0, 2\pi\right)$.

Making the assumption that the amplitude gain g_S can be considered stationary, our measurement results show that $G_S = 20\log_{10} g_S$ can be well described by a correlated Gaussian variable. This simplified approach is more appealing than that of including various ground reflections into the model; since the reflected contributions will change over time, their deterministic modeling is not straightforward. We hence analyze the distance autocorrelation function of G_S, i.e.,

$$r_d\left(\Delta d\right) = E\left\{G_{S,p} G_{S,p}^{1/2}(d + \Delta d)\right\}. \qquad (4)$$

A commonly used model for describing large-scale fading is the exponential auto-correlation function [23], but our estimated distance correlation functions (see Fig. 6) are better described by a Gaussian function

$$r_d\left(\Delta d\right) = \sigma_S^2 e^{-\frac{\ln 2}{d_{0.5}^2}(\Delta d)^2}, \qquad (5)$$

where σ_S^2 is the variance of the process and $d_{0.5}$ is the $0.5-$coherence distance defined by $r_d\left(d_{0.5}\right)/r_d\left(0\right) = 0.5$.

2) Diffuse Scatterers: The complex path amplitude of a diffuse scatterer r is modeled as in classical GSCM by

$$a_r = G_{0,\text{DI}} c_r \left(\frac{d_{\text{ref}}}{d_{T\to r} \times d_{r\to R}}\right)^{n_{\text{DI}}/2}, \qquad (6)$$

where $c_r \sim \mathcal{CN}\left(0, \sigma^2\right)$ is complex Gaussian distributed in agreement with our observations in Sec. III-A. The pathloss exponent n_{DI} and the reference power $G_{0,\text{DI}}$ are the same for all diffuse scatterers.

Our tracking algorithm only provides information about discrete scatterers and does hence not directly provide information about n_{DI} and $G_{0,\text{DI}}$. However, these parameter can be estimated by means of simulations. First, "diffuse" impulse responses are derived from the measurement data by subtracting the LOS component and the discrete components detected by the tracking algorithm of Sec. III-C. Then the rms delay spread of the measured "diffuse" channel is determined as a comparative measure. By comparing these delay spreads to those obtained from simulations according to our model, best-fit values of n_{DI} and $G_{0,\text{DI}}$ can be estimated. Due to the randomness of the measured roadside environment, the

[2]Fig. 4 seems to suggest two random processes, one slow and one fast, though the variations of the fast fluctuations are very small. However, investigations show the fast process to be highly specific for our measurement setup and it is thus not included in our model (see [20] for further details).

[3]Distinction between reflections stemming from mobile and static objects is made using their respective Doppler shifts, see Sec. III-B.

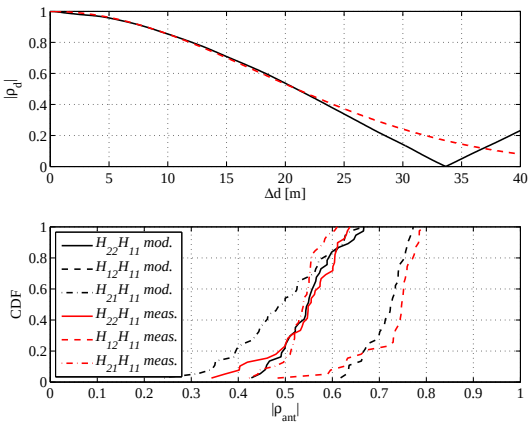

Fig. 6. Top: Large-scale distance correlation $\rho_{\mathrm{d}} = r_d(\Delta d)/r_d(0)$ for path 3 of Fig. 3 (solid) along with a fit to (5) (dashed). Bottom: CDFs of measured and simulated antenna correlation ρ_{ant} for a time window of 3 s of an SM scenario with $v_T = v_R = 50$ km/h and $d_{T\to R} = 100$ m. H_{ij} defines the channel from TX element j to RX element i and antenna elements 1 and 2 have their broadside directions at 135 and 45 degrees, respectively (see Sec. II-A).

extracted delay spreads vary within each measurement. Since such variations are not included in our model, we select the values of n_{DI} and $G_{0,\mathrm{diff}}$ that provide the best fit *on average*. This approach is similar in spirit to [24], which also extracts discrete scatterers by high-resolution algorithms, and models the remainder as diffuse components whose PDF (in the delay/angle plane) is fixed, and whose parameters are extracted from best-fit.

C. Scatterer Distributions

The number of point scatterers are derived from densities χ_{MD}, χ_{SD}, and χ_{DI}, respectively, stating the number of scatterers per meter. Then, using the geometry in Fig. 5, we model the y–coordinate of mobile discrete scatterers by a uniform discrete probability density function (PDF) where the possible number of outcomes equals the number of road lanes, N_{lanes}. Their *initial* x–coordinates are modeled by a (continuous) uniform distribution over the length of the road strip, i.e., $x_{p,0} \sim \mathcal{U}[x_{\min}, x_{\max}]$. Each mobile scatterer is assigned a constant speed along the x–axis given by a truncated Gaussian distribution (to avoid negative speeds in the wrong lane as well as too high speeds). This approach can easily be extended to include more complicated traffic models.

The x–coordinates of static discrete scatterers as well as diffuse scatterers are also modeled through $x_q \sim \mathcal{U}[x_{\min}, x_{\max}]$ and $x_r \sim \mathcal{U}[x_{\min}, x_{\max}]$. To model static discrete scatterers at either side of the road, we split the number of scatterers in two and derive separate y–coordinates for each side using Gaussian distributions $y_q \sim \mathcal{N}(y_{1,\mathrm{SD}}, \sigma_{y,\mathrm{SD}})$ or $y_q \sim \mathcal{N}(y_{2,\mathrm{SD}}, \sigma_{y,\mathrm{SD}})$, respectively (note that static scatterers in the middle of the road correspond to overhead road signs). Diffuse scatterers are also modeled on each side of the road strip; their y–coordinates are drawn from uniform distributions, over the intervals $y_r \sim \mathcal{U}[y_{1,\mathrm{DI}} - W_{\mathrm{DI}}/2, y_{1,\mathrm{DI}} + W_{\mathrm{DI}}/2]$ or $y_r \sim \mathcal{U}[y_{2,\mathrm{DI}} - W_{\mathrm{DI}}/2, y_{2,\mathrm{DI}} + W_{\mathrm{DI}}/2]$, where W_{DI} is the width of the scatterer field. Parameter values are found in Table I.

TABLE I
MODEL PARAMETERS

Parameter	Unit	LOS	MD	SD	DI
G_0	dB	-9	$-89 + 24n$		23
n		1.6	$\mathcal{U}[0, 3.5]$		3.0
μ_σ		11.7	15.1	14.8	–
μ_c	m	8.0	8.3	2.5	–
$d_c^{\min}$	m	5.4	2.5	1.4	–
χ	m^{-1}	–	0.001	0.05	1
y_1	m	–	–	-9.5	-9.5
y_2	m	–	–	9.5	9.5
W_{DI}	m	–	–	–	5
W_{road}	m	8			
N_{lanes}		2			

D. Model Parameter Statistics

Our model requires the following signal model parameters: pathloss exponents n, reference powers G_0, large-scale variances σ_S^2 and large-scale $0.5-$coherence distances $d_{0.5}$; all of which can be different for different types of scatterers. By extracting the parameters of all relevant paths using all available measurement data, we get an ensemble of results for each model parameter.[4] Based on the empirical parameter CDFs (due to space limitations we refer the reader to [20]), we find the following parameter models suitable:

- The **pathloss exponent** n is fixed for the LOS component (selected as the ensemble median value) and the diffuse scatterers. For discrete scatterers, $n \sim \mathcal{U}(0, n_{\max})$.
- The **reference power** G_0 of the discrete scatterers shows a high correlation with the pathloss exponent (~ 0.98), and is therefore modeled as a *function* of n. $G_{0,\mathrm{DI}}$ and $G_{0,\mathrm{LOS}}$ are fixed.
- The **coherence distance** $d_{0.5}$ of the stochastic amplitude process is given by an exponential distribution, though with a non-zero lowest value $d_{0.5,\min}$.
- The **variance** σ_S^2 of the stochastic amplitude process is uncorrelated with $d_{0.5}$, and given by an exponential distribution.

All model parameters are given in Table I.

V. Comparison with Measurements

The validity of the model is examined by means of comparing extensive model simulations with the measurement data.[5] The metric we use is the measured and modeled MIMO antenna correlation, i.e., we evaluate the complex correlation coefficient between every two antenna subchannels. We find the overall performance of the model satisfactory and we also note that the model outcome can vary a lot from one simulation to another; the latter being due to the non-stationary nature of the channel. Since the correlation outcome depends largely on the strength and position of the discrete scatterers, an exact

[4] Discrete parameters are only estimated from the antenna subchannel where the tracked path is the strongest and only paths spanning over a relative distance range (defined as $2(d_{\max} - d_{\min})/(d_{\max} + d_{\min})$) of more than 0.2 are considered. Furthermore, with the distance ranges over which we observe the components, the changes in angles-of-arrival and departure are usually small enough to stay within the antenna 3 dB beamwidth and we thus make the assumption of a constant antenna gain during the observation.

[5] A detailed implementation recipe of the model can be found in [20].

measure of the agreement between measurement and model is difficult to give, as the number of measurements to our disposal is relatively small in this aspect. We instead settle for showing a typical comparison plot; Fig. 6 shows a simulation of an SM scenario that is compared to a measurement with the same TX/RX speed and TX-RX separation.

Deviations between model and measurements mainly stem from the simplifications we use:

- The diffuse scatterer distribution we use in the model is uniform with a constant density over the road strip, which is a major simplification of reality where roadside sections alter between being crowded with scatterers to being completely empty.
- The TX and RX antenna patterns we use in the model simulations are calibration measurements of the arrays only, i.e., without the influence of the cars.
- The spatial distributions of the discrete scatterers are greatly simplified.

VI. Summary and Conclusions

We have presented a model that is suitable to describe the time-varying properties of a MIMO vehicle-to-vehicle propagation channel. The model is based on extensive measurements from which we noted that:

- Significant energy is available from scatterers, labeled *discrete*, such as cars, houses, and road signs on and next to the road. Their contributions typically move through many delay bins during a measurement and thus violate the commonly adopted WSSUS assumption.
- The time-varying power of discrete components and LOS is fading.
- The LOS is usually followed by a tail of weaker components, labeled *diffuse*, who give rise to Rayleigh distributed amplitude statistics in the delay bins immediately following the LOS.
- The total Doppler spread of the channel is large and the Doppler spectrum can change rapidly with time.

These observations (though here based on rural motorways, similar qualitative behavior is experienced in a highway scenario, see [20]), suggest a need for a channel model able to handle the non-WSSUS conditions typically arising in traffic environments, and for those reasons we found a geometry-based stochastic channel model (GSCM) as best suited. The assumption of single-reflection processes only keeps simulation runtimes small and thus requires a much smaller computational effort than comparable ray-tracing approaches.

Model parameters were extracted from all available measurement data using a high resolution algorithm (for signal parameters) and the measurement environment (for geometry parameters) and given as constants or statistical distributions. Finally, comparing simulations of the model to the measurement data we concluded that the model gives a good overall description of the MIMO VTV channel and can thus be used for simulations of future wireless systems.

Acknowledgments: The authors gratefully acknowledge Dr. Helmut Hofstetter for assisting during the measurements.

References

[1] J. Zhu and S. Roy, "MAC for dedicated short range communications in intelligent transport systems," *IEEE Commun. Mag.*, vol. 41, no. 12, pp. 60–67, Dec. 2003.

[2] J. H. Winters, "On the capacity of radio communications systems with diversity in Rayleigh fading environments," *IEEE J. Select. Areas Commun.*, vol. 5, no. 5, pp. 871–878, June 1987.

[3] G. J. Foschini and M. J. Gans, "On limits of wireless communications in a fading environment when using multiple antennas," *Wireless Personal Commun.*, vol. 6, pp. 311–335, Feb. 1998.

[4] P. C. F. Eggers, T. W. C. Brown, K. Olesen, G. F. Pedersen, G. Durisi, and S. Benedetto, "Assessment of capacity support and scattering in experimental high speed vehicle to vehicle MIMO links," in *Proc. IEEE Veh. Technol. Conf. 2007 spring*, Apr. 2007, pp. 466–470.

[5] M. Matthaiou, D. I. Laurenson, and C.-X. Wang, "Capacity study of vehicle-to-roadside MIMO channels with a line-of-sight component," in *Proc. IEEE Wireless Commun. Networking Conf.*, Apr. 2008, pp. 775–779.

[6] A. Paier *et al.*, "First results from car-to-car and car-to-infrastructure radio channel measurements at 5.2 GHz," in *Proc. IEEE Int. Symp. Personal, Indoor, Mobile Radio Commun.*, vol. 1, 2007, pp. 1–5.

[7] H. Asplund, A. A. Glazunov, A. F. Molisch, K. I. Pedersen, and M. Steinbauer, "The COST259 directional channel model - II. macrocells," *IEEE Trans. Wireless Commun.*, vol. 5, pp. 3434–3450, 2006.

[8] P. Almers *et al.*, "Survey of channel and radio propagation models for wireless MIMO systems," *EURASIP J. Wireless Commun. Networking*, vol. 2007, 2007.

[9] J. Maurer, "Strahlenoptisches Kanalmodell für die Fahrzeug-Fahrzeug-Funkkommunikation," Ph.D. dissertation, Institut für Höchstfrequenztechnik und Elektronik (IHE), Universität Karlsruhe (TH), Karlsruhe, Germany, July 2005, in German.

[10] J. Maurer, T. Fugen, T. Schafer, and W. Wiesbeck, "A new inter-vehicle communications (IVC) channel model," *Proc. IEEE Veh. Technol. Conf. 2004 fall*, vol. 1, pp. 9–13, Sept. 2004.

[11] G. Acosta-Marum and M. A. Ingram, "Six time- and frequency-selective empirical channel models for vehicular wireless LANs," in *Proc. IEEE Veh. Technol. Conf. 2007 fall*, Sept. 2007, pp. 2134–2138.

[12] G. Acosta-Marum and M. Ingram, "Doubly selective vehicle-to-vehicle channel measurements and modeling at 5.9 GHz," in *Proc. Int. Symp. Wireless Personal Multimedia Commun.*, 2006.

[13] J. Fuhl, A. F. Molisch, and E. Bonek, "Unified channel model for mobile radio systems with smart antennas," in *IEE Proc. Radar, Sonar Navig.*, vol. 145, Feb. 1998, pp. 32–41.

[14] P. Petrus, J. H. Reed, and T. S. Rappaport, "Geometrical-based statistical macrocell channel model for mobile environments," *IEEE Trans. Commun.*, vol. 50, pp. 495–502, 2002.

[15] A. F. Molisch, A. Kuchar, J. Laurila, K. Hugl, and R. Schmalenberger, "Geometry-based directional model for mobile radio channels - principles and implementation," *European Trans. Telecomm.*, vol. 14, pp. 351–359, 2003.

[16] A. F. Molisch, "A generic channel model for MIMO wireless propagation channels in macro- and microcells," *IEEE Trans. Signal Processing*, vol. 52, no. 1, pp. 61–71, Jan. 2004.

[17] C. Wei, H. Zhiyi, and Y. Tianren, "A street reference model of MIMO vehicle-to-vehicle fading channel," in *Proc. IEEE Conf. on Ind. Electron. Appl.*, June 2008, pp. 275–278.

[18] A. Paier *et al.*, "Non-WSSUS vehicular channel characterization in highway and urban scenarios at 5.2 GHz using the local scattering function," in *International ITG Workshop on Smart Antennas*, 2008.

[19] R. Thomae *et al.*, "Identification of the time-variant directional mobile radio channels," *IEEE Trans. Instrum. Meas.*, vol. 49, pp. 357–364, 2000.

[20] J. Karedal *et al.*, "A geometry-based stochastic MIMO model for vehicle-to-vehicle communications," *IEEE Trans. Wireless Commun.*, 2008, submitted for publication.

[21] R. J.-M. Cramer, R. A. Scholtz, and M. Z. Win, "Evaluation of an ultra-wide-band propagation channel," *IEEE Trans. Antennas Propagat.*, vol. 50, no. 5, pp. 541–550, May 2002.

[22] A. F. Molisch, *Wireless Communications*. Chichester, West Sussex, UK: IEEE Press–Wiley, 2005.

[23] M. Gudmundsson, "Correlation model for shadow fading in mobile radio systems," *IEEE Electron. Lett.*, vol. 27, no. 23, pp. 2145–2146, Nov. 1991.

[24] A. Richter, "Estimation of radio channel parameters: Models and algorithms," Ph.D. dissertation, University of Ilmenau, Ilmenau, Germany, May 2005.